JOINT INSTITUTE FOR NUCLEAR RESEARCH
Bogoliubov Laboratory of Theoretical Physics

FINAL REPORT ON THE SUMMER STUDENT PROGRAM

Structural properties of two-phase deterministic multifractal

Supervisor:
Dr. Eugen Anitas

Student:
Giorgia Marcelli, Italy
Sapienza University of Rome

Participation period:
July 30 – September 14
Dubna, 2018

Structural properties of two-phase deterministic multifractals

Abstract. This report attempts to compare the analysis of the multifractal spectra, pair distance distribution function (PDDF) and Small-Angle Scattering (SAS) intensities in order to determine structural properties of deterministic multifractals. We show that the coefficients of the PDDF are characterized by the presence of groups of distance pairs whose positions are related to the scaling factors of the fractal. We found that the box counting dimension D_0 in the multifractal spectra coincides with the fractal dimension, determined through the evaluation of scattering exponent in the fractal region of the SAS form factor. We illustrate the relevance of these results in a 2D Vicsek-like multifractal example.

1. Introduction

In the last decades and in many research fields, in particular the one concerning life sciences, the concept of fractal geometry introduced by Mandelbrot [1], acquired a strong development. Since then, in term of fractals is possible to describe and quantitatively characterize complex natural structures with irregular shapes, not eligible by Euclidean geometry. For example, trees, mountains, coasts, neurons and liver structures are just few examples of fractal structures existing in the world around us [1] [2].

Starting from the 1960s and 1970s, several independently Swiss and French research groups, discovered that biological systems show characteristics of internal statistical homothetia, i.e a transformation of the Euclidean space which dilates or contracts objects, preserving their shapes [3], and may express fractal properties within a precise range of scale. In this way it is also possible to identify specific qualities of the object observed and describe it using the fractal dimension [2].

If structures of objects in the animate and inanimate world are fractals and their homothetia is statistic, self-similarity represents an imprint of the same design, always new, but at the same time different. As a consequence, images of a respiratory or vascular networks, although similar, are never the same [4].

The fractal analysis yields to the determination of the fractal dimension, which represents an index of irregularity and complexity of the system under examination [2]. The higher is the numerical value of this parameter, the higher is the irregularity of the system and its morphologically complexity. In this way the mathematical concept of fractal geometry may then characterize and distinguish numerous biological and non-biological structures [5].

In the recent years, new experimental techniques have been developed to manufacture hierarchically organized systems, opening new opportunities to control and understand their properties and functionalities. One of the main goal of modern physics is trying to understand how the electromagnetic, dynamic and statistical properties of a fractal object are related to its micro-structures [4] [6].

Experimentally, it is possible to describe material's micro-structures using scattering techniques. In particular, a typical range used to study material's hierarchical structure is

within $10 \div 10^4$ Å, which corresponds to values of the scattering vector q within the range: $10^3 \div 0.45$ Å^{-1} [6] [7] [8]. This range of q well matches with the Small Angle Scattering technique (SAS) [9]. However, since only a finite range of scattering vector values is available experimentally, theoretical models for data interpretation are required [6] [2].

In the case of non-deterministic fractals, different models for mass and surface fractals have been developed and applied to a great variety of materials. Nevertheless, regarding deterministic fractals, only a few efforts have been made due to technological limitations for the preparation of this kind of fractal structures [6] [4].

The main features of a fractal structure can be obtained by analyzing the power law trend in the scattering intensity [9] [6] [8]:

$$I(q) \sim q^{-\alpha}, \tag{1}$$

where α is the scattering exponent, $I(q)$ is the scattering intensity and q is the scattering vector. In particular the exponent α contains informations regarding the fractal dimension of the curve. In contrast to the behavior of the power law (Eq. 1) [8], the scattering from deterministic fractals shows a sequence of maxima and minima, which follows the power law distribution, due to spatial order properties of these structures [6] [10]. The scattering intensity minima $I(q)$ are related to the missing distances of the PDDF.

In this contribution we attempt to compare different methods in order to obtain the fractal dimension of a two-phase fractal system similar to the Generalized Self-Similar Vicsek Fractal system (GSSVF) discussed in [6], composed of disks with two different scaling factors.

Classically, once the scattering intensity of a randomly oriented fractal system is analytically determined, it is possible to extract three parameters: the exponent α (Eq. 1) and the edges of the fractal region in the q space, which appear as knees in the scattering curve on a logarithmic-scale [9] [11]. As explained in section 2.3 the scattering intensity can be represented as a function of the fractal form factor, which carries information about the relative objects positions within the fractal system [9] . Analyzing these distances it is possible to extract additional informations concerning the fractal structure.

Section 2.2.1 explains how can be derived the fractal dimension from the analysis of the multifractal spectrum.

Results and discussion of the theoretical calculations performed are explained in Section 3 .

2. Theoretical background

In this section we review some important concepts concerning the technique of Small Angle Scattering (SAS), providing some numerical techniques to calculate the scattering intensity from simple geometric shapes, in particular the scattering amplitude from a sphere and from a disk. A general definition of fractals and multifractals is given, focusing in detail on the determination of the multifractal spectra through the box-counting method. In addition, to obtain informations over the objects positions within a fractal polydisperse system, some general notions concerning the pair distance distribution function are underlined.

2.1. Small angle scattering

Small angle scattering is a technique based on spatial density measurement, used to analyze structures with nano-scale sizes [9] [11] [12]. Fig. 1 shows a typical SAS experimental setup, where a beam of X-rays or neutrons strikes a sample, and it is recorded by a detector, located after the sample. In order to characterize structures down to the nanometric region, the beam must have wavelengths comparable with the atomic distances within the sample [9] [11] [13].

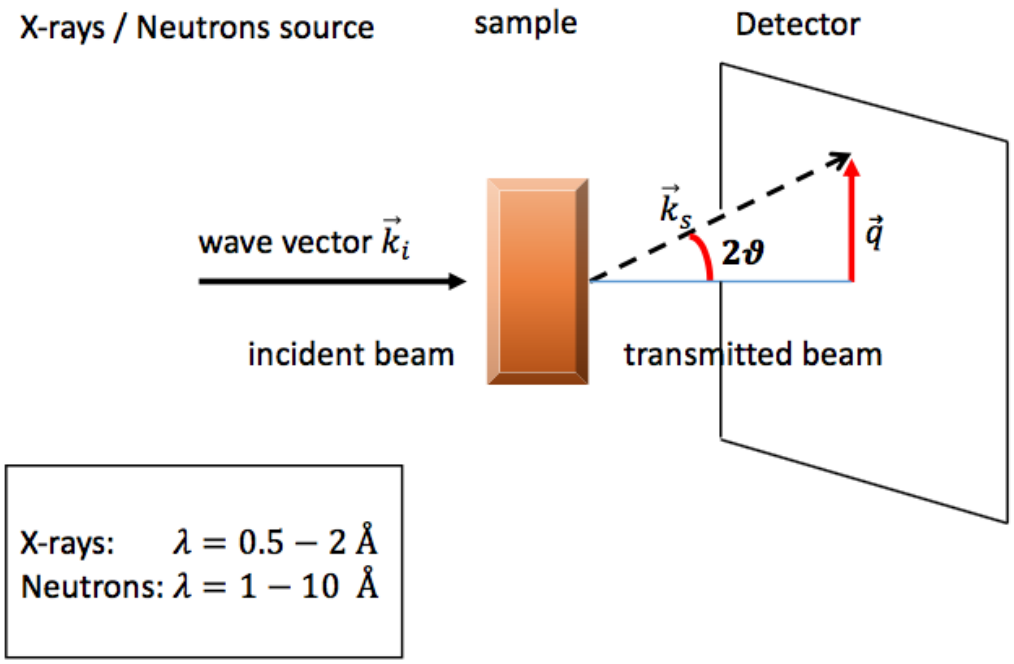

Figure 1. Synthetic representation of a Small Angle Scattering experimental setup.

Defining the wave vector of the incident beam as $\vec{k}_i$ and the wave vector of the scattered beam as $\vec{k}_s$, which makes an angle equal to 2θ with the direction of the transmitted beam, the quantity measured in a SAS experiment is the differential cross section as a function of the scattering vector $\vec{q} = \vec{k}_s - \vec{k}_i$ [9] [12]. The scattering vector $\vec{q}$ is completely characterized by the scattering geometry and its magnitude is related to the scattering angle 2θ by the following relation [9] [11] [13]:

$$q = \frac{4\pi \sin\theta}{\lambda}, \tag{2}$$

where λ is the wavelength of the incident beam. The range of q in a SAS experiment extends usually from 0.001 Å^{-1} to 0.45 Å^{-1} (see 1) and it depends on various factors, such as the beam

wavelength or the distance at which the detector is placed [6] [9] [11] [13].

Considering a sample of N identical scatters with scattering length b_j, it is possible to express the scattering length density as [6] [9] [11]:

$$\rho(\vec{r}) = \sum_j b_j \delta(\vec{r} - \vec{r_j}), \tag{3}$$

where r_j are the positions of the scatters within the sample and δ is the Dirac's delta function. Then, the amplitude of the scattered beam can be written as [6] [9] [11]:

$$A(\vec{q}) = A_0 \sum_{j=1}^{N} \rho(\vec{r}) e^{-i \cdot \vec{q} \cdot \vec{r_j}}, \tag{4}$$

where the summation is usually replaced with an integral when the system consists of a very large number of scatters, dispersed continuously within the sample.

Thus, the total scattering amplitude results to be proportional to the Fourier transform of $\rho(\vec{r})$ [9] [11] [12]:

$$A(\vec{q}) = A_0 \int_V \rho(\vec{r}) e^{-i \cdot \vec{q} \cdot \vec{r}} d\vec{r}, \tag{5}$$

where V denotes that the integration as to take place over the scattering volume.

During the time period of scattering measurements, the positions $\vec{r_j}$ of atoms and the scattering length density distribution $\rho(\vec{r})$ may change due to thermal motion of the atoms. Therefore, the resulting intensity is measured as the average over the time [9] [11].

Thus, it is more appropriately to write Eq. 5 as [6] [9] [11] [12] [13]:

$$I(q) = \langle |A(q)|^2 \rangle = \langle | \int_V \rho(\vec{r}) e^{-i\vec{q} \cdot \vec{r}} d\vec{r} \quad |^2 \rangle = V^2 \langle |F(\vec{q})|^2 \rangle, \tag{6}$$

where the $\langle ... \rangle$ denotes the ensemble average and $F(\vec{q})$ is the normalized scattering amplitude, given by [6] [9] [11] [12] [13]:

$$F(\vec{q}) = \frac{1}{V} \int_V \rho(\vec{r}) e^{-i\vec{q} \cdot \vec{r} d\vec{r}}. \tag{7}$$

2.1.1. Scattering from a sphere and from a disk: As a first example, it is possible to derive the scattering intensity of a ball with unit density, radius R and volume $V = \frac{4}{3}\pi R^3$. In the first step, it is necessary to rewrite the normalized scattering amplitude (Eq. 7) in spherical coordinates [9] [11]:

$$F(\vec{q}) = \frac{1}{V} \int_{\phi=0}^{2\pi} \int_{\theta=0}^{\pi} \int_{r=0}^{\infty} \rho(r) e^{-i\vec{q} \cdot \vec{r}} r^2 \sin\theta dr d\theta d\phi, \tag{8}$$

where:

$$\rho(r) = \begin{cases} 1 & \text{if } r < \text{R} \\ 0 & \text{if } r > \text{R} \end{cases} \tag{9}$$

Choosing the polar axis coinciding with the vector $\vec{q}$ direction, we obtain [9] [11]:

$$\vec{q} \cdot \vec{r} = qr \cos\theta. \tag{10}$$

By denoting $u = \cos\theta$, Eq. 8 becomes [9] [11]:

$$F(q) = \frac{1}{V}\int_{\phi=0}^{2\pi}\int_{\theta=0}^{\pi}\int_{r=0}^{\infty}\rho(r)e^{-iqru}r^2\sin\theta dr d\theta d\phi = \frac{1}{V}\int_{r=0}^{R}4\pi r^2\frac{\sin(qr)}{qr}dr. \tag{11}$$

Resolving the expression through the integration by parts, the normalized scattering amplitude of the sphere is equal to [9] [11] [13]:

$$F(qR) = 3\frac{\sin(qR) - (qR)\cos(qR)}{(qR)^3}, \tag{12}$$

and the resulting scattering intensity becomes [9] [11] [13]:

$$I(q) = |F(qR)|^2 = 9\frac{\Big(\sin(qR) - (qR)\cos(qR)\Big)^2}{(qR)^6}. \tag{13}$$

The second example concerns a disk of radius R and area $S = 4\pi R^2$, for which it is possible to derive the total scattering intensity in a similar way as the previous method. Denoting $\vec{q} = \{q_x, q_y\}$ and $\vec{r} = \{x, y\}$, the normalized scattering intensity is given by [9] [11] [13]:

$$F(\vec{q}) = \frac{1}{S}\int_{-\infty}^{+\infty}\int_{-\infty}^{+\infty}\rho(r)e^{-i\cdot\vec{q}\cdot\vec{r}}d\vec{r}. \tag{14}$$

Passing to a spherical coordinates system, where [9] [11]:

$$\begin{cases} q_x = \rho_0\cos\phi \\ q_y = \rho_0\sin\phi \end{cases} \tag{15}$$

and:

$$\begin{cases} x = r\cos\theta \\ y = r\sin\theta \end{cases} \tag{16}$$

$F(\vec{q})$ can be expressed as:

$$F(\rho_0, \phi) = \frac{1}{S}\int_0^{2\pi}\int_0^{+\infty}\rho(r,\theta)e^{-i\rho_0 r\cos(\phi-\theta)}r dr d\theta. \tag{17}$$

Since $\rho(r,\theta)$ is [9] [11] [14]:

(i) separable in spherical coordinates, $\rho(r,\theta) = \rho(r)\rho(\theta)$,
(ii) circularly symmetric, $\rho(\theta) = 1$,

the normalized scattering amplitude $F(\rho_0, \phi)$ is equal to [9] [11] [14]:

$$F(\rho_0, \phi) = \frac{2\pi}{S}\int_0^{+\infty} r\rho(r)dr\left(\frac{1}{2\pi}\int_0^{2\pi}e^{i\rho_0 r\cos(\theta-\phi)}d\theta\right), \tag{18}$$

where [14]:

$$J_0(\rho_0, r) = \frac{1}{2\pi}\int_0^{2\pi}e^{i\rho_0 r\cos(\theta-\phi)}d\theta \tag{19}$$

is the zero order Bessel function of the first kind. Then [9] [11] [14]:

$$F(\rho_0,\phi) = \frac{2\pi}{S}\int_0^{2\pi} r\rho(r)J_0(\rho_0 r)dr = \frac{2\pi}{S}\int_0^{1} rJ_0(\rho_0 r)dr, \tag{20}$$

replacing $r' = \rho_0 r \rightarrow dr' = \rho_0 dr$ and $0 \leq r' \leq \rho_0$, we obtain [9] [11] [14]:

$$F(\rho_0,\phi) = \frac{2\pi}{S}\int_0^{\rho_0} \frac{r'}{\rho_0}J_0(r')\frac{dr'}{\rho_0} = \frac{2\pi}{S\cdot\rho_0^2}\int_0^{\rho_0} r'J_0(r')dr', \tag{21}$$

which, taking advantage of the Bessel functions properties, yields to [14]:

$$F(\rho_0,\phi) = \frac{2\pi}{S\cdot\rho_0}J_1(\rho_0). \tag{22}$$

The total scattering intensity is therefore obtained [9] [11] [14]:

$$I(q) = |F(q)|^2 = \frac{1}{4\pi R^2}\frac{J_1^2(q)}{q^2}. \tag{23}$$

Fig. 2 shows SAS scattering intensity of a sphere of radius $R = 1$ nm (Eq. 13) and of a disk of radius $R = 1$ nm (Eq. 23) represented in a double logarithmic scale. It is possible to distinguish two main regions: the Guinier region and the Porod one. For very small values of q ($q < \frac{\pi}{R}$) the curve is a plateau (Guinier region), with $I(q) \propto q^0$, which provides informations about the overall structure of the sample [8] [9] [11] [12] [13]. As q increases the curve falls off, following a power-law decay, denoted as Porod law (Eq. 1) where the exponent α is equal to 4, when the system consists of spheres (three dimensional), is equal to 2 for disks (two dimensional), and so forth [8] [12] [13]. In particular, it is possible to notice that in Fig. 2 the SAS intensity of a sphere presents many peaks in the Porod region, while the disk intensity is represented as a straight line. The lack of peaks in the disk intensity curve is due to the fact that we calculated the average of the normalized scattering amplitude over the whole solid angle (3D space) [13]. The same function averaged over the 2D plane yields to a curve made by maxima and minima, as the one shows in Fig. 2 for the sphere.

2.2. Fractals and multifractals

A fractal is an object which exhibits dilatation symmetry, that is a self-similarity property under scale transformations [1] [2]. A real object can be a fractal only within a range of values imposed by its effective physical dimension and by the size of the basic building blocks of its structure [1] [2] [9]. The most important characteristic of a fractal is its *fractal dimension d*.

The meaning of this quantity can be explained considering a sphere of radius r around a point inside the object, taken into account. If the fractal object is a line (1D) the mass $M(r)$ within the sphere will be proportional to r; if the fractal is a sheet then $M(r) \propto r^2$ and so forth [1] [2] [8] [10] [13]. Hence, fractal objects follow this general relation:

$$M(r) \propto r^d. \tag{24}$$

where $1 < d < 3$ and it is usually called Hausdorff -Besicovitch dimension [1] [2]. Some fractal structures are constructed by using an iterative process consisting of an initiator and a generator (iterative operation). The fractal dimension d may be found directly from a single iteration if the limit structure is a known fractal. Therefore, if a fractal of size L with mass $M(L) = A(L)L^d$, after some iterations, gives k elements of size $\frac{L}{\beta_s}$, it is possible to determine its dimension d [1] [2]:

$$M(L) = nM\left(\frac{L}{\beta_s}\right) \rightarrow A(L)L^d = kA\left(\frac{L}{\beta_s}\right)\left(\frac{L}{\beta_s}\right)^d. \tag{25}$$

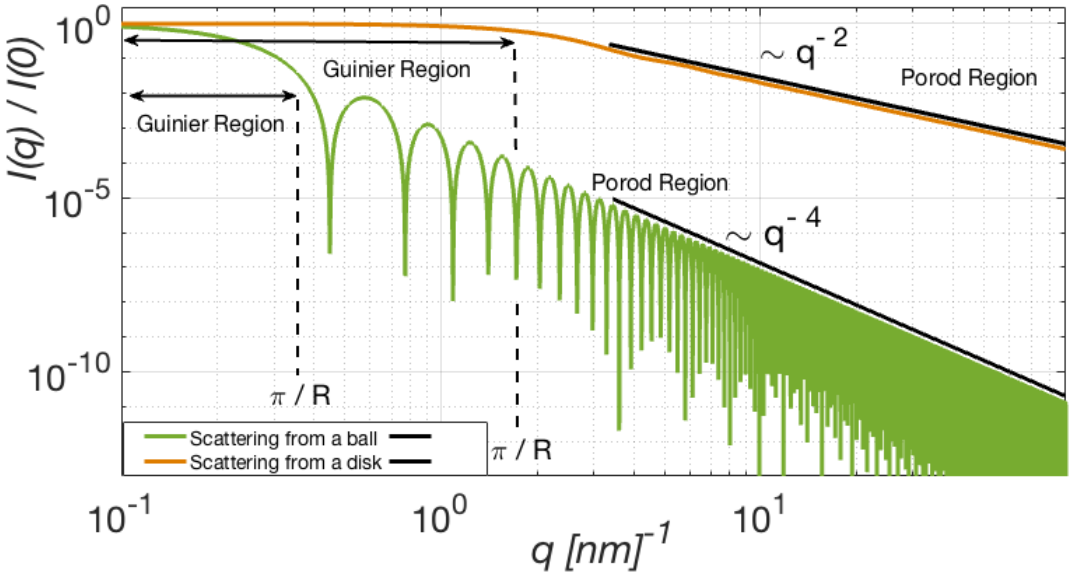

Figure 2. SAS intensity from a sphere of radius R=1 nm from Eq. 13 (green curve) and SAS intensity from a disk of radius R=1 nm from Eq. 23 (orange curve).

Taking into account that [1] [2]:

$$\frac{(\frac{L}{\beta_s})}{A(L)} \to 1 \quad as \quad L \to \infty, \tag{26}$$

It is possible to determine asymptotically d (when $L \to \infty$) from [1] [2]:

$$k\left(\frac{1}{\beta_s}\right)^d = 1. \tag{27}$$

When the iterative operation yield to a fractal structure with elements of different sizes $\frac{L}{\beta_{si}}$ $(i = 1, ..., n)$ it is possible to determine the fractal dimension through the same procedure introduced above [1] [2]:

$$M(L) = k_1 M\left(\frac{L}{\beta_{s1}}\right) + k_2 M\left(\frac{L}{\beta_{s2}}\right) + ... + k_n M\left(\frac{L}{\beta_{sn}}\right), \tag{28}$$

which means that the mass of the fractal of size L is the sum of k_i masses of similar fractals of sizes $\frac{L}{\beta_{si}}$. Then, it is possible to determine d from [1] [2]:

$$k_1\left(\frac{1}{\beta_{s1}}\right)^d + k_2\left(\frac{1}{\beta_{s2}}\right)^d + ... + k_n\left(\frac{1}{\beta_{sn}}\right)^d = 1. \tag{29}$$

Since a fractal object consists of an ensemble of fractal supports, whose fractal dimension generally differs from that of the whole, knowing the fractal dimension of a set is usually insufficient to characterize its geometry and any other physical phenomenon occurring on it [1] [2] [5] [6] [7]. Thus, in order to understand physical systems with multiple scaling factors (known as multifractals), it is necessary to characterize the distribution of measures inside

the system [5] . Multifractals objects deal with the concept of measure. In order to explain multifractal physical system let us consider a subset $D \subset \mathbb{R}^n$ on which are defined [5]:

- a fractal measurement method $\mathcal{M}$;
- a finite measure μ which we want to study.

A multifractal measure μ on D is characterized by a distribution such that around any $x \in D$, the measure in a ball of radius R around x scales with R, i.e. $x \propto R^{\alpha}$,and it is such that the sets (formed by all points around which the scaling exponent α is the same) are monofractals for $\mathcal{M}$.

2.2.1. Box-counting method Multifractal spatial data and image analysis can be performed throughout many ways. Most of the methods are based in counting the measure at different levels of aggregation. Aggregation is realized applying square grids (or other unit shapes) of increasing resolutions to the data (box-counting). Box-counting techniques are used for 'static' measures but they are not applicable to nonconservative phenomena, such as turbulence velocity profiles.

Let us consider a grid of unit R covering a domain D and a phenomenon occurring k times in D and define the probability that an instance of the phenomenon occurs in the i^{th} box as [1] [2] [5]:

$$p_i = \frac{k_i}{k} = \int_{i^{th}box} d\mu(x), \tag{30}$$

where μ is the corresponding probability measure. In particular:

- $p_i \sim R^{\alpha_i}$,
- $k(\alpha_i) \sim \rho(\alpha_i) d(\alpha_i) r^{-f(\alpha_i)}$,

where $k(\alpha_i)$ is the number of times α falls in each interval $[\alpha_i, \alpha_i + d\alpha_i]$ and ρ is a density function used to take into account the dimension of D. To estimate f it is generally used the momentum methods. Considering [1] [2] [5] [6] [13]:

$$Z(q) = \sum_i p_i^s \sim \sum_i R^{\alpha_i s} \sim \int_{\alpha} k(\alpha) R^{\alpha \cdot s} \sim \int \rho(\alpha) R^{-\alpha \cdot s \cdot f(\alpha)} d\alpha, \tag{31}$$

for small R, the value of $Z(s)$ is given by the value of α for which: [2] [5]

$$\tau(s) = \alpha s - f(\alpha) \tag{32}$$

is minimal.

Performing a Legendre transform it is possible to show that the minimum condition yields to [2] [5]:

$$\alpha(s) = \frac{s\tau(s)}{ds}, \tag{33}$$

and:

$$f(\alpha(s)) = \alpha(s)s - \tau(s). \tag{34}$$

Then, the the generalized dimension D_s is related to the scaling function $\tau(s)$ by the following relation [5] [6] [13] [?]:

$$D_s = \frac{\tau(s)}{s-1}. \tag{35}$$

Three values of the generalized dimension are of particular interest:

- D_0, which is the usual box-counting dimension of D;
- D_1, denoted as the *information dimension*, which is related to Shannon's entropy (higher values of D_1 mean a more uniform density);
- D_2, which is the probability of pairs of independent events occurring in the same box and measures how scattered the data is.

The plot of D_s over s represents the strength of the multifractality nature of μ. If the plot tends to be a straight line, then the multifractal system tends to be a monofractal. Hence, it helps us to analyze the multifractal distribution of objects [5].

2.3. Pair Distance Distribution Function

Through the pair distance distribution function method it is possible to obtain precise structure and size informations about the object we are going to analyze [6] [8]. The PDDF yields to the probability of finding pairs of atoms separated by a distance r. Considering a monodisperse fractal, composed of N disks of the same radius, the general expression of the *form factor* can be written as [6]:

$$S(q) = 1 + \frac{2}{N} \sum_{1<k<j<N} \frac{\sin qr_{jk}}{qr_jk}, \tag{36}$$

where $r_{jk} = |r_j - r_k|$ are the distances between the disk centers of the fractals. Taking into account that the sum could contain equals term, as the distances separating different points can coincide, it is necessary to introduce the probability density of finding two arbitrarily disks inside the fractal at distance r [6] [7] [8] :

$$p(r) = \frac{2}{N(N-1)} \sum_{k<j} \delta(r - r_{jk}) = \frac{2}{N(N-1)} \sum_{r_p} C_p \delta(r - r_p), \tag{37}$$

where C_p are the numbers of distances separated by r_p. Eq. 36 is called *pair distance distribution function*. By using Eq. 36and 37, one can obtain the following results [6] [7] [8]:

$$S(q) = 1 + (N-1) \int_0^{+\infty} drp(r) \frac{sinqr}{qr}. \tag{38}$$

By performing the inverse Fourier sine transform, we obtain [6] [7] [8]:

$$p(r) = \frac{2}{\pi} \int_0^{+\infty} \frac{S(q) - 1}{N-1} qr \sin qrdq. \tag{39}$$

3. Results and discussions

3.1. Theoretical model

We focus here in the construction a fractal system similar to a Generalized Self-Similar Vicsek Fractals (GSSVF), discussed in [6]. Our fractal initiator consists of a disk placed inside a square of edge l_0. In order to obtain the first iteration we choose a Cartesian system whose origin coincide with the center of the square and we built the fractal replacing the initial disk with five other disks. Defining the radius of the fractal initiator as:

$$r_0 = \frac{l_0}{2}, \tag{40}$$

the central disk will have a scaling factor equal to:

$$\beta_{s2} = \frac{r_1}{r_0}, \tag{41}$$

where, r_1 stands for its radius. While, the other four disks will have a scaling factor equal to:

$$\beta_{s1} = \frac{r_2}{r_0}, \tag{42}$$

where r_2 stands for their radius. The central disk will be located in the center of the square, while the other four disks will be shifted from the origin by the vectors:

$$a_j \equiv \vec{\beta_t} = (\beta_t, \beta_t) = \left(\frac{\beta_{s1} + \beta_{s2}}{2}, \frac{\beta_{s1} + \beta_{s2}}{2} \right). \tag{43}$$

The next iteration are obtained by carrying out the same procedure to each disks of the first iteration and so forth for the other iterations.

Performing this mathematical procedure for $\beta_{s1} = 0.45$ and $\beta_{s2} = 0.1$, at the first, second and third order iteration respectively, we obtained the following three fractal-like systems:

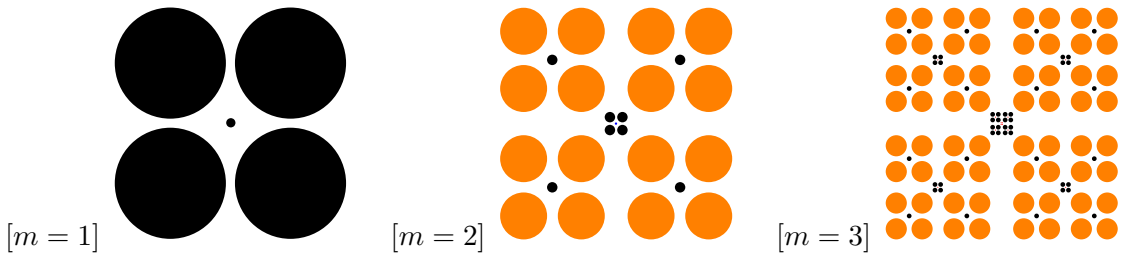

Figure 3. Three first iteration of two scale multifractals model for $\beta_{s1} = 0.45$ and $\beta_{s2} = 0.1$

3.2. Fractal form factor

Taking into account the previous mathematical procedure to generate a fractal system, it is possible to calculate analytically the form factor of the *mth* generation throughout the so called *Generative Function* $G_m(q)$, defined by the disks centers positions. From the generative function for a GSSVF system at the *mth*, defined in [6],it is possible to derive the generative function for our system taking into account the presence of two scaling factors.

Assuming $G_0(q) = 1$, it is possible to express the form factor as [6]:

$$F_m(q) = F_0(r_m q) \prod_{i=0}^{m} G_i(q), \tag{44}$$

for $m = 0, 1, 2, ...$

Hence, SAS intensity is obtained [6]:

$$\frac{I_m(q)}{I_m(0)} = \langle |F_m(q)|^2 \rangle. \tag{45}$$

In Fig. 4 we show the numerical results obtained for a 3^{rd} order fractal system scattering intensity. In the curve it is possible to distinguish three regions: the Guinier, the fractal and the Porod regions [7] [8] [9] [11] [12]. The Guinier region is presented as a plateau and provides general information about the overall structural properties of the fractal, as discussed in section 2.1.1 [8] [9].

The fractal region is determined by the maximal and minimal distances between the disks centerers and, as it is clearly shown in Fig. 4,that it follows a power-law decay in which the absolute value of the scattering exponent coincides with the fractal dimension of the system. The length of the fractal regime increases with increasing the iteration number, since the distances between the scattering units of the fractals decrease [6] [8] [13].

In Fig. 4 the fractal regime is clearly seen within the range $10 < q < 100$ for $m = 3$. It is characterized by a succession of maxima and minima superimposed on a power-law decay (Eq. 1). Beyond the fractal regime, one obtain as expected, the Porod region where the exponent of the power-law decay is $\alpha = 3$, i.e the scattering intensity is equal to the one of the initiator. In Fig. 4 the Porod regime begins near $q > 10^2$.

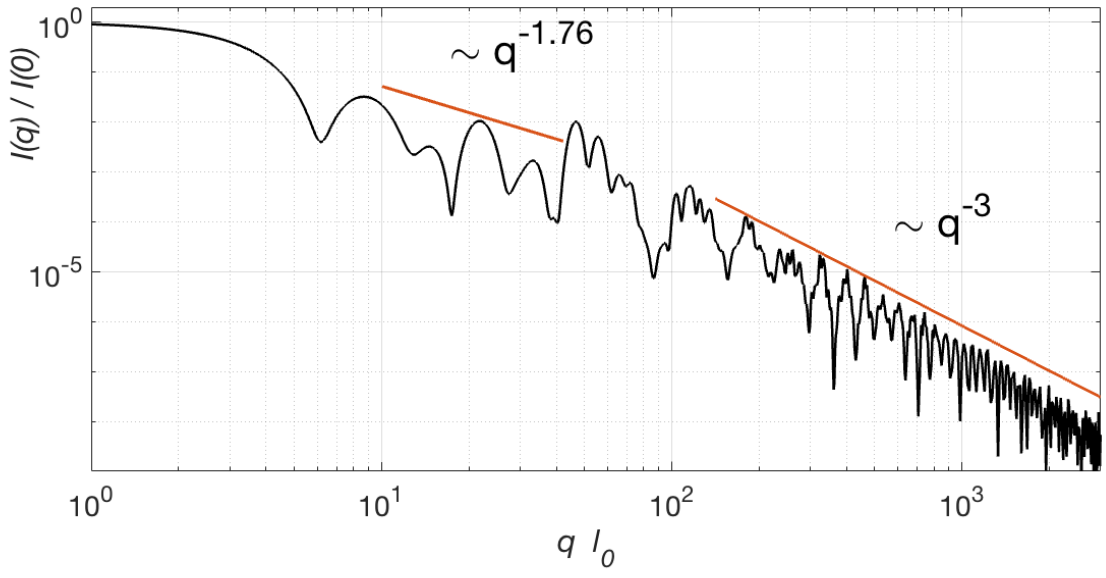

Figure 4. Scattering intensity of the 3th order iteration of the two-phase deterministic GSSVF fractal system

3.3. Pair distance distribution function

Analytically computing the PDDF, through methods explained in section 2.3, we found a simple way to determine the scaling factors of our fractal system and the order of iteration of the analyzed system.

For a system at the fourth order iteration, we shown that the coefficients of the PDDF are characterized by the presence of groups of distance pairs whose positions are related to the scaling factors of the fractal. In particular the ratio between each pairs of minima, with good approximation, coincides with the smallest scaling factor β_{s2} of our fractal system.

In our case, having considered a system that presents a very high dimensional homogeneity (see Fig. 3) , the resolution of the minima is not trivial.

However,in Fig. 5 it is possible to distinguish four main minima:

$$\left(\frac{r}{l_0}\right)_1 \approx 2.5 \cdot 10^{-3}, \tag{46}$$

$$\left(\frac{r}{l_0}\right)_2 \approx 2.5 \cdot 10^{-2}, \tag{47}$$

$$\left(\frac{r}{l_0}\right)_3 \approx 2.5 \cdot 10^{-1}, \tag{48}$$

$$\left(\frac{r}{l_0}\right)_4 \approx 2.5 \cdot 10^{0}, \tag{49}$$

where the subscript coefficients $(1-2-3-4)$ indicate respectively order of the minima. The ratio between Eq. 47 and Eq. 46, Eq. 48 and Eq. 47, Eq. 49 and Eq. 48 coincides with the scaling factor β_{s2}. It is possible to further deduce that the number of minima presented in Fig. 5 coincides with the iteration order of the fractal.

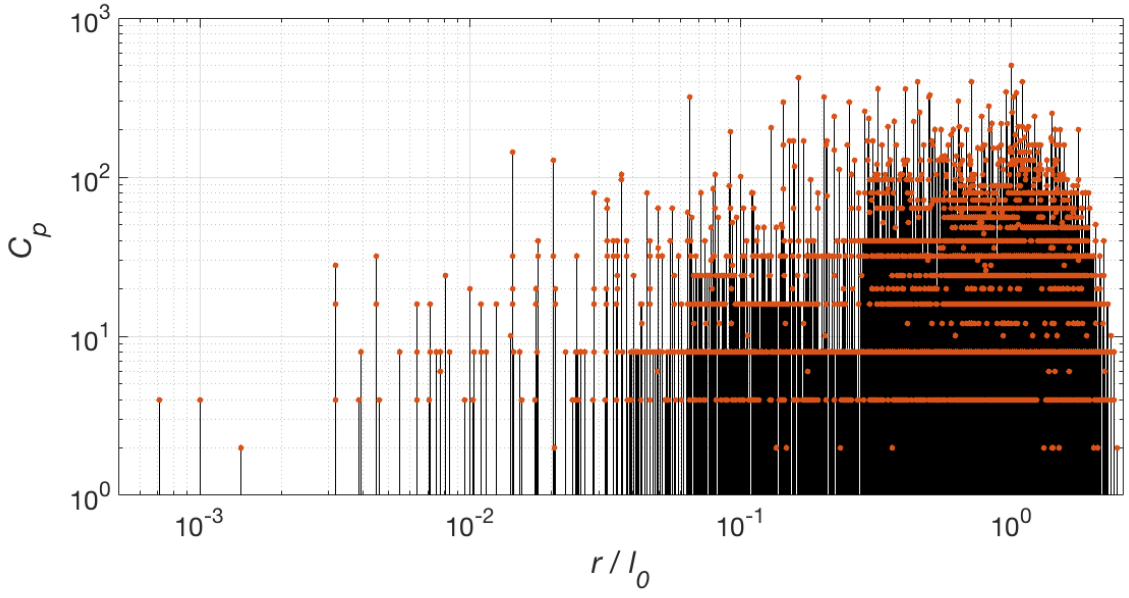

Figure 5. The coefficients C_p in the expression 36 for the pair distribution function of the analyzed fractal system at the 4th iteration. (m=4, $\beta_{s1} = 0.45$, $\beta_{s2} = 0.1$, $D = 1.76$)

3.4. Multifractal spectra

Analyzing the multifractal spectra numerically performing the box-counting method we obtained the trend of the generalized dimension D_s (Fig. 6). As stated in section 2.2.1, from Fig. 6, it is possible to obtain general information regarding the multifractal nature of the system. The spectrum presented in Fig. 6 is almost a straight line, underlining the high dimensional homogeneity of the system, also found in the PDDF distribution. This means that our multifractal can be considered, with good approximation, as a mono fractal. Moreover, it can be seen that the average of the box counting dimension D_s in the multifractal spectra approximately coincides with a straight line whose value is $D_0 = 1.76$. This value is exactly equal to the fractal dimension, determined both theoretically (Eq. 29) and through the evaluation of the scattering exponent in the fractal region of the SAS form factor(Sec. 3.2).

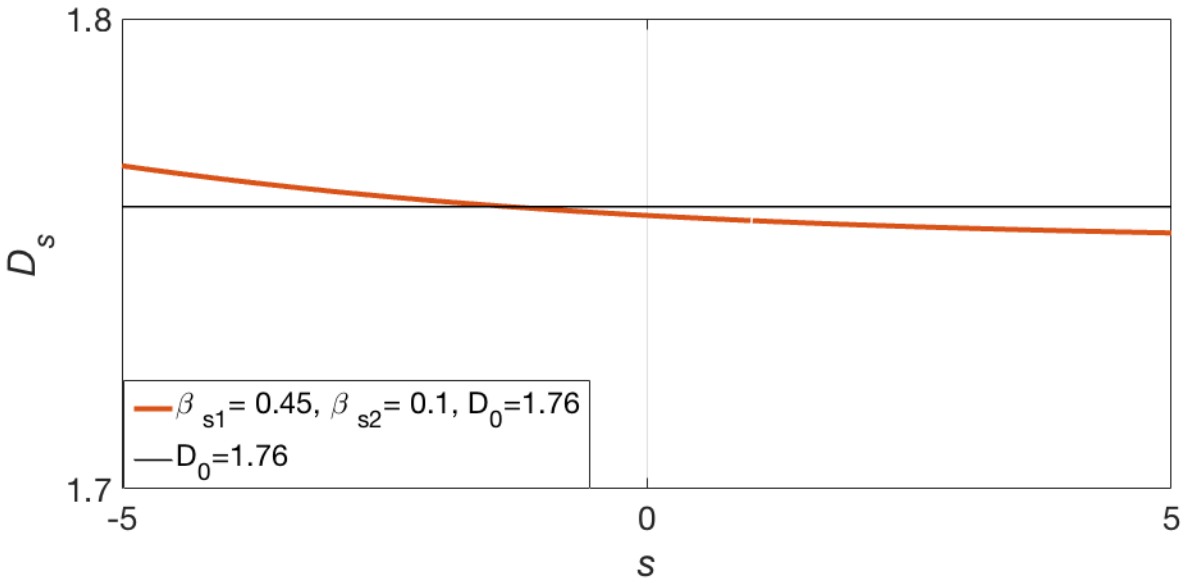

Figure 6. Trend of the generalized dimension D_s (Eq. 35) over s (Eq. 2) for the investigated multifractal system.

Conclusions

In this contribution we have presented and discussed a theoretical model which describes small angle scattering intensity from a deterministic two phase multifractal system. The model is a two dimensional system whose basic building units are disks. The latter are distributed as to form a fractal system similar to the GSSVF presented in [6]. The two scaling factors of the system are $\beta_{s1} = 0.45$, for the external disks, and $\beta_{s2} = 0.1$ for the central disk.

Based on this model we calculated the fractal form factor and we shown that this can be characterized by the presence of tree main regions: at low q the Guinier region which gives informations about the overall sizes of the fractal, at intermediate values of q the exponent of the scattering vector coincides with the fractal dimension D_0 of the system $D_0 = 1.76$, while at high values of q the scattering intensity decays following the Porod law behavior(Eq. 1).

Analytically computing the PDDF function we demonstrated that it is possible to numerically determine the smallest scaling factor β_{s2} by analyzing the ratio between the function minima. Moreover, we deduced that the number of minima coincide with the iteration order of the system itself.

Performing a multifractal spatial analysis through the box-counting method we shown that the trend of the generalized dimension D_s over the values of s provides informations about the multifractality nature of the system. The model analyzed in particular tends to be a straight line, denoting that our multifractal system appears as a monofractal. Moreover, we found that the value of the generalized dimension D_s for $s = 0$ coincides with the fractal dimension obtained from SAS data.

The results point out a number of general features, common for deterministic mass fractals with two scaling factors, which can be used to understand experimental data and can be generalized for fractal systems with more than two scaling factors. For the analyzed system it is possible to extract several information from the scattering intensity, the PDDF function and from the generalized dimension spectra:

(i) the the fractal dimension from the generalized power law;

(ii) the fractal scaling factors from the period of the minima pairs in the PDDF distribution;

(iii) the number of fractal iterations, which is equal to the number of periods in the PDDF distribution;

(iv) the multifractality nature of the system and the fractal dimension of the system itself from the multifractal spectra.

The results obtained can be applied for various structures, whose geometries are based on iterations of fractal systems, like magnetic cluster structures, chemical compounds artificially assembled, and so forth. We consider mass fractals composed of the same units, but the developed approach can be used also for mass fractal systems containing units of various shapes and sizes and to surface fractals as well.

Acknowledgment
I would like to thank the organizers of Summer Student Program for providing education opportunities and valuable experiences through being part of JINR community.

Thanks to University Center staff for their assistance in solving all the issues and a special thank to JINR for the financial support.

I think I could not have been more lucky. Every day I spent here I had the opportunity to learn new things. My work has been a constant inspiration and I do not know how to express all the gratitude I feel towards my supervisor. He has always been patient and kind to me, and most of all, he taught me to look at the reality that surrounds me with different eyes.

Thank you Prof. Eugen.

References

[1] B.B. Mandelbrot, *The Fractal Geometry of Nature* (W. H. Freeman, 1983).

[2] J.F. Gouyet, *Physics and Fractal Structure* (MASSON, 1996).

[3] E.B. Meserve, *Homothetic transformations - Fundamental Concepts of Geometry* (Addison-Wesley,1955)

[4] B.L. Su, C. Sanchez, X.Y. Yang *Hierarchically Structured Porous Materials* (WILEY-VCH, Germany)

[5] H. Salat, R. Murcio, E. Arcaute, *Multifractal methodology* Physica A-online journal (2017) **473**, 467-487.

[6] A.Yu Cherny, E.M. Anitas, V.A. Osipov, A.I Kuklin, *Deterministic fractals: Extracting additional information from small-angle scattering data*, Physical Review E (2011), **84**, 036203.

[7] G. Franceschetti, D. Riccio, *Scattering, Natural Surfaces and Fractals* (Elsevier Inc., 2007)

[8] P.W. Schmidt, *Small Angle Scattering Studies of Disordered, Porous and Fractal System* Journal of Applied Crystallography (1991) **24**, 414-435.

[9] R. J. Roe, *Methods of X-Rays and Neutron Scattering in Polymer Science* (Oxford University Press, USA, 2000)

[10] A.Y. Cherny, E.M. Anitas, V.A. Osipov, A.I. Kuklin, *Small-angle scattering from the Cantor surface fractal on the plane and the Koch snowflake* Phys. Chem. Chem. Phys. (2017) **19**, 2261-2268 .

[11] L.A. Feigin, D.I. Svergun *Structure Analysis by Small-Angle X-Ray and Neutron Scattering* (Springer Science+Business Media New York,USA, 1987)

[12] H. Brumberger, *Modern Aspects of Small-Angle Scattering* (Springer Science+Business Media New York, LLC, USA)

[13] A.M.Slyamov, E.M. Anitas, *Chaos Theory* (K.A.M. Al Naimee, Intech Open, 2018)

[14] M. Abramowitz, I. Stegun, *Handbook of Mathematical Functions* (Dover Publications, NY, 1970).

[15] G. Wilfried, *Particle and particle systems characterization* (CRC press, USA)

[16] G.F. Cerofolini, D. Narducci, P. Amato, E. Romano, *Fractal Nanotechnology* Nanoscale Research Letters (2008) **3**, 381.